Hindawi Publishing Corporation
Journal of Marine Biology
Volume 2009, Article ID 861590, 11 pages
doi:10.1155/2009/861590

Research Article

Computational Assessment of the Fluid Flow around Coasting Mature Male Blue Sharks, *Prionace glauca* (L.)

T. H. E. Smith[1,2] and G. S. Caldwell[1]

[1] *School of Marine Science and Technology, Newcastle University, Ridley Building, Claremont Road, Newcastle Upon Tyne, Tyne and Wear, NE1 7RU, UK*
[2] *School of Biological Sciences, University of Aberdeen, Tillydrone Avenue, Aberdeen AB24 2TZ, UK*

Correspondence should be addressed to T. H. E. Smith, tsmith@abdn.ac.uk

Received 1 July 2009; Accepted 28 October 2009

Recommended by Garth L. Fletcher

Body-induced vortices and flow regimes surrounding five mature male blue sharks, *Prionace glauca* (L.), were investigated. Flow was simulated using 3-dimensional computational fluid dynamics software (*Fluent*). A *k*-epsilon turbulent model represented the ocean flow regime. Compared to controls (horizontal cylinders) morphology increased the flow velocity along the body surface. The region around the gill slits displayed maximum relative velocity magnitude which may improve oxygen uptake. The area of the lateral line adjacent to the dorsal fin returned the minimum relative velocity magnitude. The vorticity magnitude was enhanced by dorsal fin-body interactions along the adjacent section of lateral line suggesting that *P. glauca* channels vortices along the lateral line, at reduced relative velocity magnitudes.

1. Introduction

Fish have evolved specific morphological adaptations to enhance swimming efficiency that combine hydrodynamic performance and functional biology [1]. In fish, body form is critical for vortex creation and control. Vortices formed at the body anterior alter the turbulence profile available for manipulation by the caudal fin [2] which will affect propulsion and wake components. There have been a number of recent studies (e.g., [3–6]) investigating how fish maintain stability and utilise vortices when moving through areas of unpredictable turbulence. Locomotion control and vortex generation mechanisms other than the fins include, for example, the development of specific morphological features such as the keels and ridges associated with the carapace of tropical boxfish.

The blue shark, *Prionace glauca* (L.), is classed as a body and caudal fin (BCF) swimmer [7]—a fish that moves body and caudal fin to transfer momentum to the surrounding water through lift, drag, and acceleration. *P. glauca* utilises the subcarangiform swimming mode whereby the posterior half of the body, including the dorsal fin, undulates [8]. Undulatory swimming creates both forward thrust and lateral force components that act to displace water sideways. It is thought that the lateral force is a cause of significant energy loss [9] but that it may have a stabilising role. In *P. glauca* this lateral water mass effect and associated energy loss is reduced by the flattened head which, in addition to its lift generating role, would also compensate for the large lateral movements undertaken by the dorsal fin as part of subcarangiform swimming. Webb [8] suggested that the main role of the dorsal fin was to reduce yaw and roll by producing lateral drag. The tensile strength of the dorsal fin can be altered through hydrostatic pressure changes [10] so that strength correlates with swimming speed. This allows efficiency in both slow and fast swimming [10] and the ability to counterbalance the increased yaw and roll motions at higher swimming speeds. *P. glauca,* being primarily oceanic, is highly migratory in nature [11] but does also spend a large proportion of its time in inshore areas [12]. This may have influenced its morphological evolution due to the higher proportion of turbulent flows in coastal waters and the associated requirement for greater manoeuvrability.

Burst-and-coast swimming allows the body to be rigid for half of the two-phase swimming mode thereby reducing frictional drag [1]. Coasting occurs when the body remains straight and forward motion continues through momentum alone. During coasting, vortex production occurs anterior to the caudal fin due to a combination of body form, boundary layer separation, and fin edge effects [2]. Sparenberg [13] described how energy lost to the surrounding fluid in the form of kinetic energy could be recovered by the manipulation of these anterior vortices by the caudal fin during active swimming. In this way vortex control and manipulation may provide an energy conservation mechanism during long migrations [14].

In pelagic sharks, respiration and forward momentum are inextricably linked. Gill ventilation is achieved via ram ventilation at swimming speeds above a threshold value and is enhanced at low speeds by branchial pumping [15]. In fast swimming sharks in particular, it may be assumed that body form has evolved to contribute towards maximisation of ram ventilation efficiency. Similarly, body form should have a pivotal role in informing the evolution of dermal-associated sensory structures such as the ampullae of Lorenzini and the mechanosensory lateral line system. The combined sensory function of the ampullae of Lorenzini [16] and the lateral line system [17] allow *P. glauca* to detect prey and other organisms within its environment [18] and undertake extensive rheotaxis-guided migrations [19]. The lateral line is composed of superficial neuromasts, which sense lower-frequency vibrations, and canal neuromasts, for higher frequencies [20]. Fish that are active swimmers generally have fewer superficial neuromasts and narrower canals [19]. The narrower canals are more efficient at filtering out lower frequency background noise created by ambient water movement [21]. Superficial neuromasts may also be more susceptible to damage by fast flowing currents due to the more exposed nature of the associated hair cells. Body form may enhance lateral line sensitivity by redirecting flow across it in a similar fashion that variation in elasmobranch dermal denticle morphology creates an anterior-posterior channelling of water towards the pit organ openings [22].

Current work has adopted a computational fluid dynamics approach to investigate morphometric-induced vortex production and the effects of the dorsal fin on flow regime in coasting mature male *P. glauca*. In particular, the flow regime in the region of the gill slits was assessed for its effect on ram ventilation. The stabilisation of flow along the lateral line by dorsal fin-body interactions and the associated benefits to the sensitivity of the lateral line are discussed.

2. Methods

2.1. Morphometry. During August 2007, measurements were taken from mature male blue sharks landed from a recreational fishery in Nova Scotia, Canada [23]. Five specimens of total length approximating to 3 m and subsequently categorised as specimens A–E were selected using the criteria of lack of injury with minimal degree of body deformation post capture and noneverted stomachs. Body length measurements (Figure 1(a)) were recorded along the midline from the tip of the snout to the fork of the tail; dorsal and ventral measurements were taken from the midline starting at the tip of the snout at 0.3 m intervals terminating at the caudal peduncle. Lateral measurements to the left and right of the midline were taken in the same way, using a right angle ruler. The midline was used to note the position of all fins along the body. The fins were traced on to laminated A3 graph paper and their widths recorded at the base and tip of both leading and trailing edges using Vernier callipers. A curve tracer was used to describe the body curvature fore and aft of the dorsal fin, around the central gill slit and at the caudal peduncle.

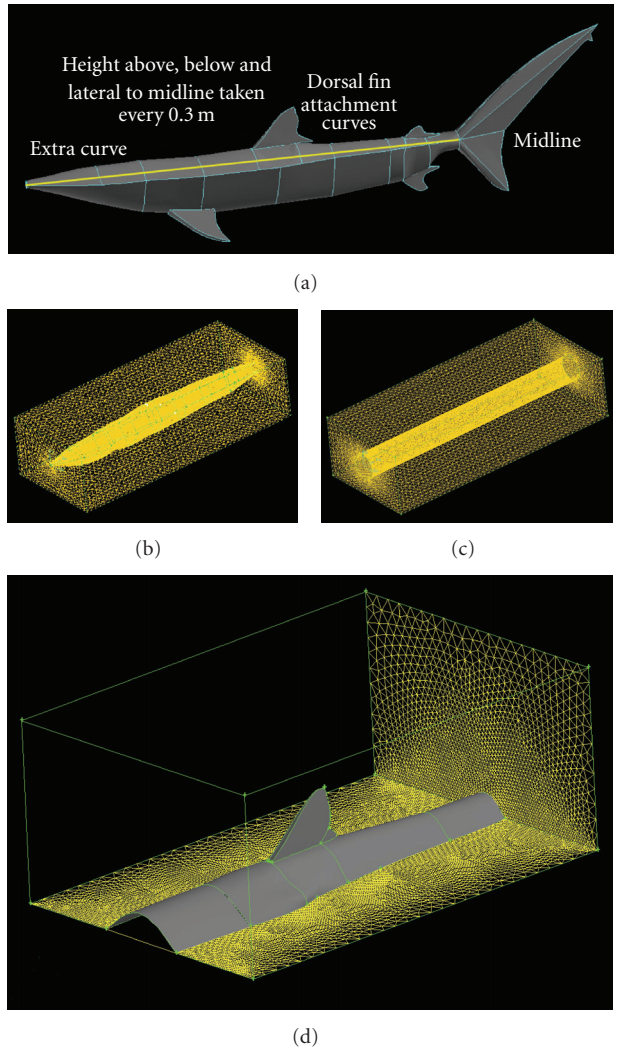

Figure 1: (a) Specimen A displayed in *Gambit* describing the measuring method used and all fin morphologies within the 3-dimensional Cartesian axis. *Gambit* meshed volumes of (b) specimen E (body section) and (c) specimen E (body section) control (cylinder e). (d) Dorsal fin section model (specimen E) displaying the cut away mesh regime of the flow tank walls and the shark dorsal section model with dorsal fin attached.

2.2. Computational Fluid Dynamics Model. Morphometric data was input into the meshing software *Gambit* using

Cartesian coordinates with the x-axis positioned along the middle of the shark body from the tip of the snout (0,0,0) to the middle of the peduncle where the y-axis described the height of the shark and the z-axis described the width (Figure 1(a)) to produce a set of vertices. Lines connecting the vertices were used to create faces along the body of the shark model and over the fins. A cuboid was created around the shark to represent a flow tank of dimensions 0.6 $\times$ 1 m along the y- and z-axes in the model simulation. The volume between the flow tank and the shark model could not be meshed due to software limitations caused by the 3-dimensional geometric complexity.

2.3. Effects of Body Form on Flow. To assess the flow along the shark body the geometry was simplified by removing all fins so the volume between the flow tank and shark body models could be meshed. An unstructured TGrid mesh (tetrahedral/hybrid) was used with an interval size of 1 at the shark body expanding to 5 at the edges of the flow tank (Figure 1(b)). The unstructured grid enabled the creation of a volumetric mesh conforming to the shark body thus permitting a more accurate shark representation. The meshes were exported into *Fluent* and run using the turbulent model k-epsilon renormalized group method (RNG) at 10 m s^{-1} along the positive x-axis over 100 iterations. The k-epsilon RNG turbulent model was chosen as it was found to have a good response to the streamline curvature and produced relatively stable turbulence. A velocity of 10 m s^{-1} was chosen to simulate *P. glauca* deceleration during coasting following an estimated maximum burst swimming speed event of 11 m s^{-1}. This velocity, although apparently high, does reside within the documented limits of *P. glauca* burst swimming speed [24, reference 25]. Other estimates of shark burst speed may be rather conservative due to limitations of the tracking methods employed [25]. Additionally, the animal would experience the straightest body profile during the high-speed coasting phase. As part of method development, prototype models were run through *Fluent* at a range of velocities. No significant differences were found between 2 and 12 m s^{-1} (data not shown). Controls were run to account for software-induced error by comparing shark models (A–E) to cylinders (a–e) of the same length (snout to caudal peduncle) and radius equal to the maximum radius of each shark (Figure 1(c)).

2.4. Dorsal Fin-Body Interactions. The effect of the dorsal fin on vortex creation along the lateral line was assessed using dorsal fin sections of the five sharks. These consisted of dorsal body sections from x = 60 cm to the start of the secondary dorsal fin, with rectangular flow tanks created around them as before (Figure 1(d)). These sections were run in *Fluent* both with and without the dorsal fin attached. Controls were created using half cylinders of length equal to the specimen dorsal fin section and run with and without each dorsal fin, specific to the specimen. Comparing control results to model results accounted for some of the error in the turbulent model so that the effect of the dorsal fin on vortex creation could be more accurately assessed. The error in the turbulent model is systemic due to the formulation used by *Fluent* to create the model.

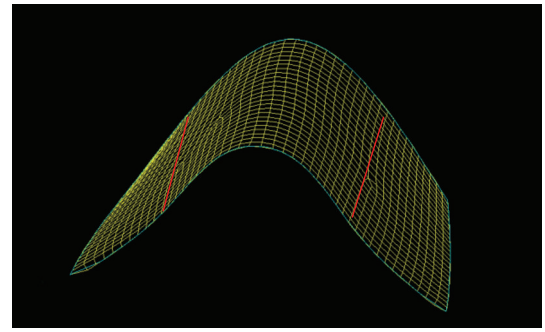

Figure 2: Dorsal surface (specimen D) immediately fore of the dorsal fin describing the "bell shaped" curve. Red lines indicate the approximate position of the lateral line.

2.5. Data Analysis. The statistical packages SPSS (v. 15) and Minitab (v. 15) were used for analysis. A Kolmogorov-Smirnov normality test was performed on all data including morphometric and that produced by *Fluent*. In the one case where data was nonnormal, a Friedman test was performed. Normal data was analysed by paired t-tests.

3. Results

3.1. General Morphology. There existed a degree of variation in body form between the five specimens including a varied rate of body tapering with lateral tapering particularly extreme in specimens B and D. This variation in lateral tapering around the dorsal fin was reflected in the results of the dorsal fin sections in *Fluent* showing individuality between the specimens.

The length distribution between fins was proportional to the total length of each shark. The distribution of total length was not significantly different from the normal distribution (Kolmogorov-Smirnov test, P = .13) and all subsequent results were normal unless otherwise indicated. Significant correlation was found between the total length of each specimen and the length to the central gill slit (R^2 = 0.676), dorsal fin (R^2 = 0.744), secondary dorsal fin (R^2 = 0.991) and caudal peduncle (R^2 = 0.986).

A particularly interesting feature present in all five sharks was the bell-shaped curvature formed in the z-y plane by the dorsal side of the body between the gill slits and immediately aft of the dorsal fin (Figure 2). This was more pronounced in specimens B and D which also showed more enhanced lateral body tapering. This curvature best fitted 4th-order polynomial equations. The lateral lines were located within the concave area of the curve as illustrated in Figure 2.

3.2. Body Morphology Results. The velocity magnitude along the shark body models was highly variable (Figure 3). Maximum velocity magnitudes occurred in all specimens in the gill slit region and reduced velocity magnitudes were described along the position of the lateral line (Figure 4). The

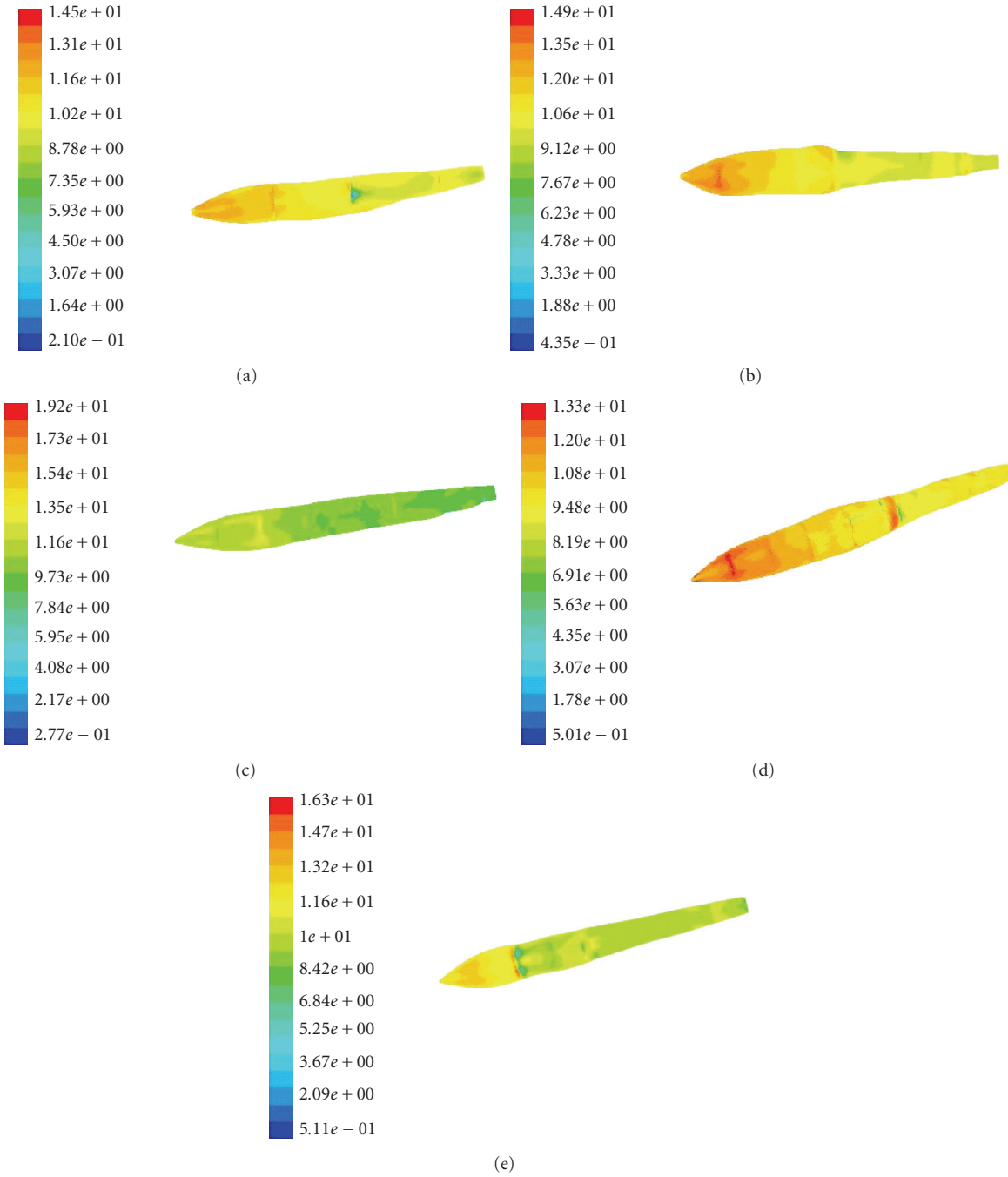

Figure 3: Dorsal aspect of shark body models (a)–(e) showing the degree of variation in velocity magnitude ($\mathrm{m\,s^{-1}}$) along the model length. Maximum velocities were observed around the gill slits with reduced velocities along the position of the lateral line. Note the variation in colour scale.

k-epsilon turbulence model created high turbulence at the inlets of all models; however, little change in flow velocity was observed in the controls (data not shown). A significant difference was found between the mean velocity of control models and shark body models, particularly in the region of the gill slits ($P < .001$) and along the lateral line of the body models ($P = .002$). A significant difference ($P = .003$) was also found between the velocities along the lateral line compared with velocities associated with the gill slit region in the shark models.

The turbulent kinetic energy produced along the central gill slit position of each shark was statistically higher than its respective control (paired t-test, $P < .001$). The vorticity magnitude was larger and more variable along the shark models than in the controls (Figure 5), with spikes in fin and gill slit positions.

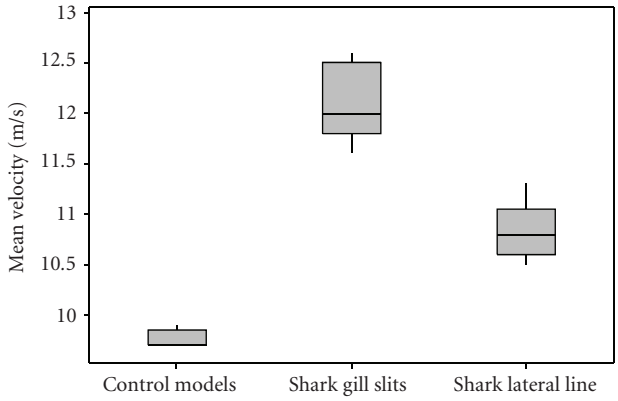

Figure 4: Mean velocity magnitude in the gill slit and lateral line regions of shark body and control models.

It is seen that, relative to the rest of the body, along the lateral line the velocity magnitude and turbulent kinetic energy decrease and the vorticity magnitude increases. The decrease in turbulent kinetic energy along with the increase in vorticity suggests that the shark body is "channelling" the water flow into vortices. This channelling effect can be seen in the bunching of the pathlines in the body models along the lateral line position (Figure 6) with a similar but much reduced effect in control models.

3.3. Dorsal Fin Section Results. Figure 7 indicates that the dorsal fin reduces the velocity along the lateral line adjacent to the fin. No statistical difference was found between the mean velocity along the lateral line in the shark and control models when the dorsal fin was not present (paired t-test, $P = .382$). However, a difference ($P = .02$) was found between shark and control models when the dorsal fin was attached. A further paired t-test shows a significant difference ($P = .001$) between the mean velocity found at the position on the lateral line adjacent to the trailing edge of the dorsal fin on shark body models with and without the dorsal fin present (Figure 7).

Figure 8 shows the difference in mean turbulent kinetic energy (k) in the dorsal section models of each specimen and its respective control, with and without the dorsal fin attached. A positive difference on this figure represents a higher turbulent kinetic energy (k) found when the dorsal fin was not attached to the model and a negative difference represents a higher turbulent kinetic energy (k) found when the dorsal fin was attached.

Whereas a higher turbulent kinetic energy was found in all shark models without dorsal fins (compared to shark body models with dorsal fins), a paired t-test found no statistical difference ($P = .067$). There was also no significant difference between control models with or without dorsal fins (paired t-test, $P = .814$). The control model for specimen E showed an opposing trend to the other specimens (Figure 8).

Figure 9 shows the vorticity magnitude produced on the surface of all shark dorsal section models where the dorsal fins are attached. The vorticity spiked to a maximum in each dorsal fin attached model at the trailing edge of the fin, as expected from the turbulence model, due to shear. The vorticity magnitudes at the dorsal fin spike on the controls were nonnormally distributed (Kolmogorov-Smirnov test, $P < .01$); therefore a Friedman test was applied. Whereas the vorticity maximum appears to be higher in the shark models than the control models, the median difference is not significantly different from zero ($P = .18$). The deviation from the normal distribution could be due to the different vortical characteristics seen in specimen E. When run without specimen E, the Friedman test showed a significant difference between the maximum vorticity at the trailing edge of the dorsal fin in the shark models compared with the controls ($P = .046$).

4. Discussion and Conclusions

Skin friction, form drag, and induced drag produce a force that acts to oppose the direction of swimming [9]. Form drag is caused by flow distortion around fish bodies and induced drag is produced due to energy losses through vortex formation behind lift or thrust generating fins. These reduce skin drag optimisation in a "performance trade-off" [1] between hydrodynamics and biological function where the need for features, such as gill slits, on the skin surface will have increased local drag. Therefore, an evolutionary driver for streamlining in fast swimming pelagic sharks will be the requirement to unify drag minimisation with the shape and positioning of external morphological features.

The common characteristics of the *P. glauca* body plan along with the small standard deviation in the body lengths of the five specimens allowed for direct comparison between sharks. However, each shark was required to be treated as an individual during statistical analysis.

The comparison between shark body models and their controls showed the significant increase in velocity magnitude that occurred at the shark body surface due to the morphological characteristics of the *P. glauca* body. This illustrates the importance of the fusiform shape (the manner in which the body radius increases from the snout to the middle of the body and then tapers off towards the tail) and the described bell-shaped dorsal profile (Figure 2).

Sparenberg [13] discusses the importance of snout morphology in creating an anterior suction force. Figure 4 illustrates the flow acceleration produced by the snout creating a velocity maximum around the gill slits. A faster flow and therefore greater turbulence in this region will enhance ram ventilation and act to increase the difference in oxygen partial pressure between the seawater and blood. This will increase oxygen uptake efficiency in a similar way to the counter current blood flow [15]. In this way, the positioning of the gill slits in the area of maximum flow velocity is an evolutionary adaptation that increases respiratory efficiency.

The reduction in mean velocity magnitude along the lateral line is seen as an adaptation to enhance lateral line functionality. An overly fast flow could damage the superficial neuromast cells thereby reducing functionality by inhibiting sensitivity in the lower frequency range. The

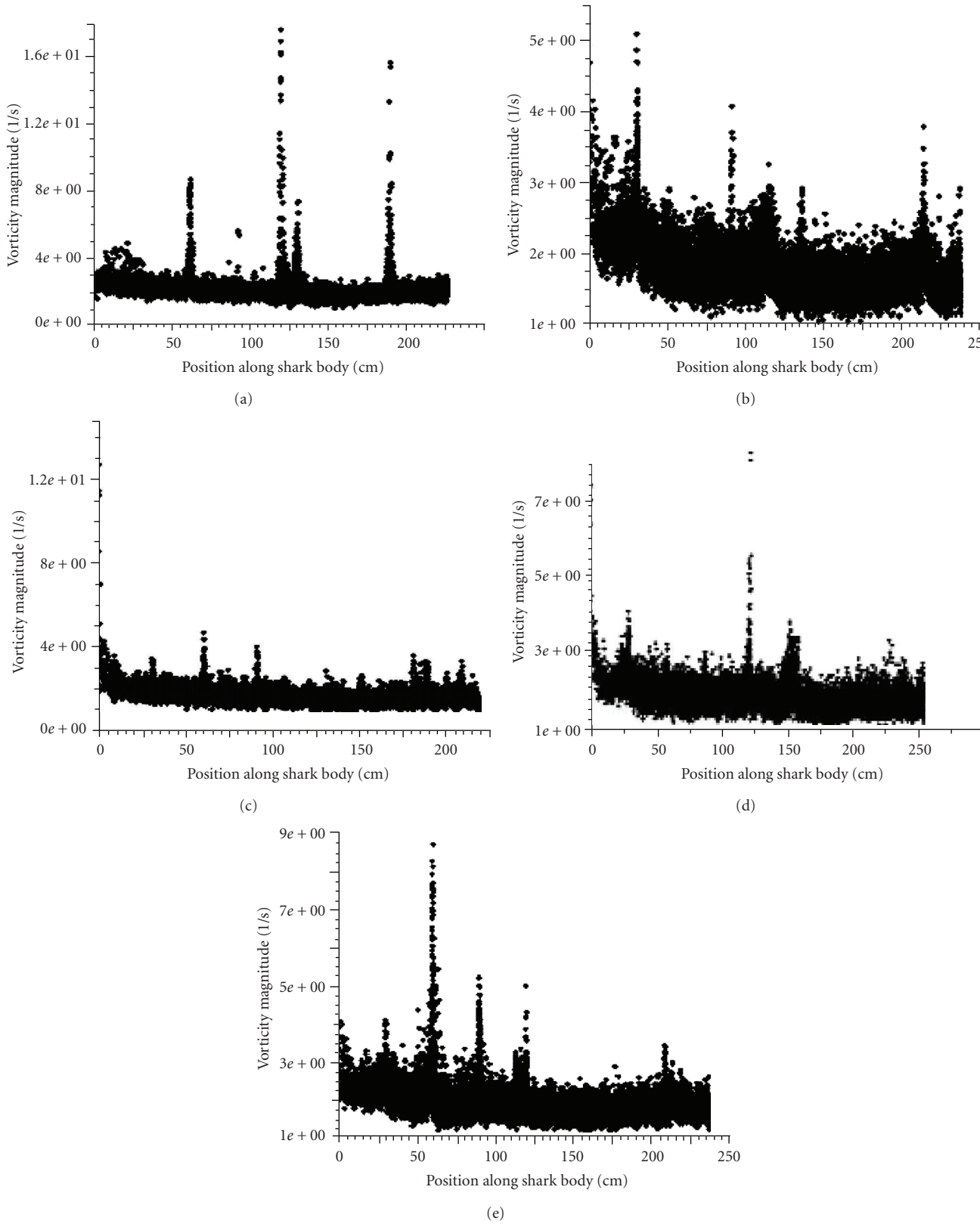

Figure 5: Vorticity magnitudes (1/s) of shark (a)–(e) body models. The x-axis on the figure represents the y-axis along the shark body models (nose to fork in the tail) and the y-axis shows the vorticity magnitude at every position on the shark at that particular y value. In this way, the figure shows the maximum vorticity magnitude at each position along the shark body model, clearly illustrating spikes of vorticity at the position of the gill slit and fins.

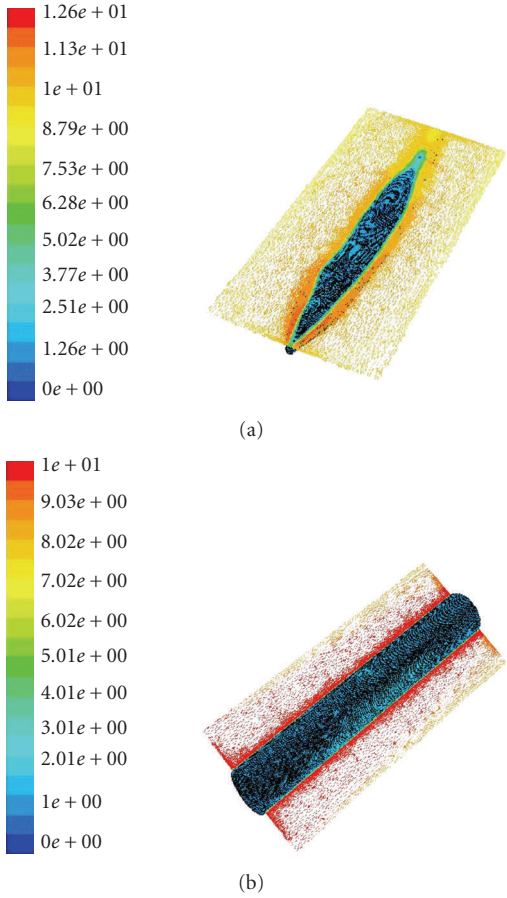

Figure 6: (a) Pathlines in the x-z plane along the lateral line of the body models of specimen A showing the channelling of the flow along the lateral line and the reduction in velocity magnitude. (b) Pathlines in the x-z plane along the equivalent position of the lateral line in specimen A for the control cylinder "a" showing the reduced bunching effect of the pathlines near the model surface due to boundary layer effects alone (pathlines coloured by velocity magnitude, m s^{-1}).

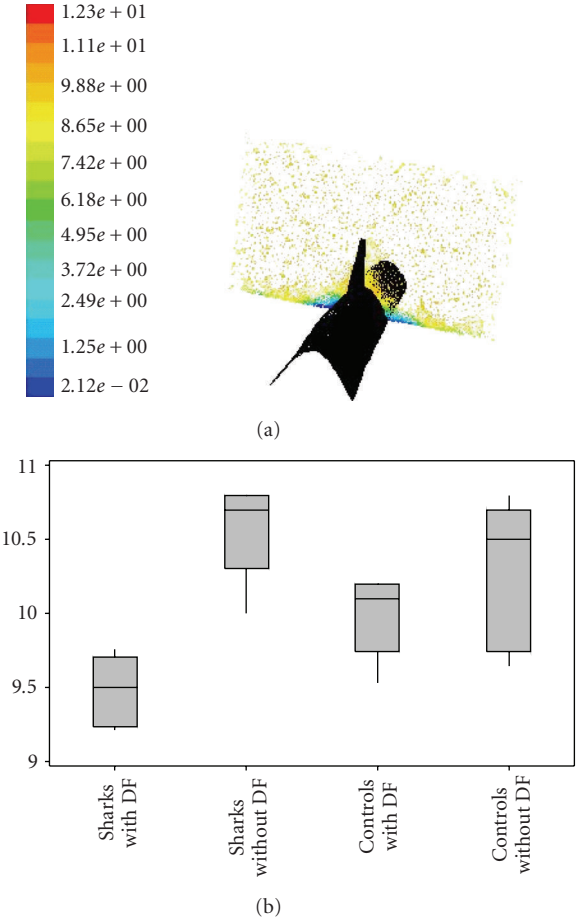

Figure 7: (a) Velocity vectors (coloured by magnitude in m s^{-1}) around the dorsal fin section of specimen C (with dorsal fin attached). Reduced velocities were described along the lateral line adjacent to the trailing edge of the fin. (b) Mean velocity along the lateral line adjacent to the trailing edge position of the dorsal fin (DF) in shark body and control models with and without the dorsal fin attached.

reduction in relative velocity magnitude along the lateral line may therefore serve a protective function.

The vorticity on the shark body surface was considerably larger than that on control models, clearly indicating body induced vorticity. A spike in vorticity was evident in the dorsal fin position of each shark body model (Figure 5) although the magnitude of the response varied both in absolute terms and relative to the vorticity spike at the gill slit position. All shark body models expressed multiple spikes in various positions along the body that in the most part correspond to areas of high shear and at fin positions (primary and secondary dorsal, anal and pectoral fins). The vorticity spikes in the positions of the absent fins suggest that the presents of fins act to reduce the vorticity (so their absence in the models produces a vorticity spike).

The results show that, along the lateral line, the velocity magnitude and turbulent kinetic energy are decreased whilst the vorticity magnitude is increased. It is thought that the increasing vorticity causes energy dissipation which acts to

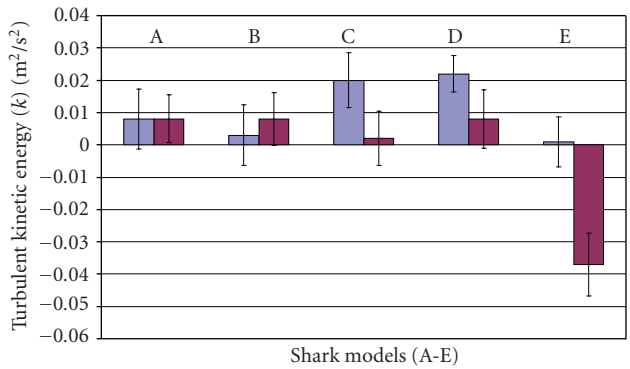

Figure 8: Difference in mean (± St Err) turbulent kinetic energy (k) between models with and without the dorsal fin attached. The light series show the results for the shark body models and the dark series show the results for the control models. A positive difference indicates a higher turbulent energy without the dorsal fin attached.

reduce the velocity magnitude. The decrease in turbulent kinetic energy along with the increase in vorticity suggests that the morphology is channelling the water flow into vortices. A similar effect was observed along the ventro-lateral keels of boxfish by Bartol et al. [3]. This channelling effect can be seen graphically in the pathlines in the body models along the lateral line position (Figure 6(a)). A similar effect is seen in control models (Figure 6(b)) but this is solely due to the boundary layer effect and therefore shows a much reduced bunching of the pathlines and does not affect the velocity magnitude. Research into the exact nature of shark skin boundary layer effects will need to be carried out before this near-body flow can be accurately measured [26, 27]. The complex nature of *P. glauca* skin surface will have hydrodynamic properties that will create a highly complex boundary layer. Anderson et al. [27] highlighted the fact that the complex and dynamic nature of fish boundary layers has so far prevented them from being accurately measured and is the reason why boundary layer effects have not been modelled separately in this current work.

Figure 7(b) illustrates the difference in mean velocity magnitude along the lateral line adjacent to the dorsal fin position in models with and without the dorsal fin. Flow fields from the dorsal fin and body morphology interact constructively to enhance the reduction in velocity caused by the presence of the dorsal fin. Figure 7(a) shows this reduced velocity (relative to the velocity over the gill slits as shown in Figure 4) but also illustrates an area of flow separation along the body on the $y = 0$ plane. This suggests that body morphology in this region of the lateral line acts to prevent flow separation, although boundary layer effects would impact this.

The prevention of flow separation along the lateral line (Figure 7(a)) would also aid its functionality. The resultant constant flow of water from fore to aft of the lateral line would act as a steady baseline flow induced by the motion of the shark. Higgs et al. [20] showed that sharks are able to cancel out the predictable self-induced flow using the octavolateral nucleus; so the reduction of turbulence over the lateral line would facilitate this physiological mechanism and thus increase lateral line efficiency. This may also explain why the lateral line is situated just above the $y = 0$ plane. This positioning would be particularly important when the shark was actively swimming as the flow separation effects would be greater, in spite of being temporally variable with regards to the movements associated with active swimming. This baseline flow would produce a similar effect for the electromagnetic sensitivity of the ampullae of Lorenzini.

There was little difference between the magnitude of turbulent kinetic energy in shark body models and controls at the high turbulence spectrum (data not shown). This may be due to the fact that the higher turbulence magnitudes were created at the inlet by the turbulence model and were quickly dissipated by both models [28]. High turbulence was created by the body form in areas of high shear and in the areas of the gill slits and at the dorsal fin. The high turbulent kinetic energy (k) associated with the position of the gill slits is due to the high velocity magnitude in this region and the nature of the calculation for k. The high turbulent kinetic energy (k) associated with the body morphology around the position of the dorsal fin is supported by the results from dorsal section models. The difference between k in models with and without the dorsal fin attached suggests that body morphology produces a larger kinetic turbulent energy in this region to counteract turbulence produced by the dorsal fin [29]. When the dorsal fin is removed, a high (effectively over-compensatory) turbulence is seen as a result of body morphology. This suggests that the turbulence created by the dorsal fin may have contributed towards the evolution of the body morphology to produce counteracting turbulence so that destructive interference (annihilation; [29]) reduces the net turbulent kinetic energy that would otherwise produce a drag force and reduce swimming efficiency.

Barrett et al. [30] showed that drag reduction in actively swimming fish (as opposed to straight bodied fish) was observed in a robotic bluefin tuna (*Thunnus thynnus*) at particular Strouhal numbers. They hypothesised that these Strouhal numbers correlated with the optimal ability of the "fish" to control body produced vorticity with the caudal fin. However, this method was unable to identify the exact origin of the vortices within the wake. Due to the difficulties in analysing wake components, sequential removal of fins during investigation of flow regime could assist in the assessment of their individual effect on the flow thus providing a useful analytical technique.

These observations clearly illustrate the importance of body morphology for influencing and directing the flow regime. This in turn suggests that studies which approximate body shape, such as in the design of RoboTuna [30], will grossly miscalculate the near-body flow regime. Naturally, the analysis of body models which have had the fins excluded does not in itself represent a true flow regime; however, this approach which was similarly adopted by Bartol et al. [3] does serve to illustrate the fundamental importance of body form.

Müller and van Leeuwen [31] suggested that convergent evolution of fish morphology may occur in species exhibiting the same swimming mode. For example, the convergent evolution with respect to body shape and swimming mode between lamnid sharks and tunas has been highlighted on a number of occasions [32, 33]. Our finding, combined with the findings of Barratt et al. [30] showing that drag reduction in RoboTuna only occurred at certain Strouhal numbers, suggests a baseline optimum morphology for a specific swimming mode. Sparenberg [13] provides a mathematical basis for optimum swimming motion; however Sfakiotakis et al. [9] highlight that whilst highly efficient swimming has evolved, it is not necessarily optimal for locomotion due to compromise with regard to the particular life history or adaptation to a specific habitat or environment. Therefore, it may be prudent to question whether any morphological form should be described as optimal due to the enormous variability of function with respect to, for example, life history and swimming mode. Despite this, analysis of morphological similarities between species that utilise the same swimming mode may show that certain body forms produce specific vortices and turbulence profiles that through manipulation by the caudal fin during active

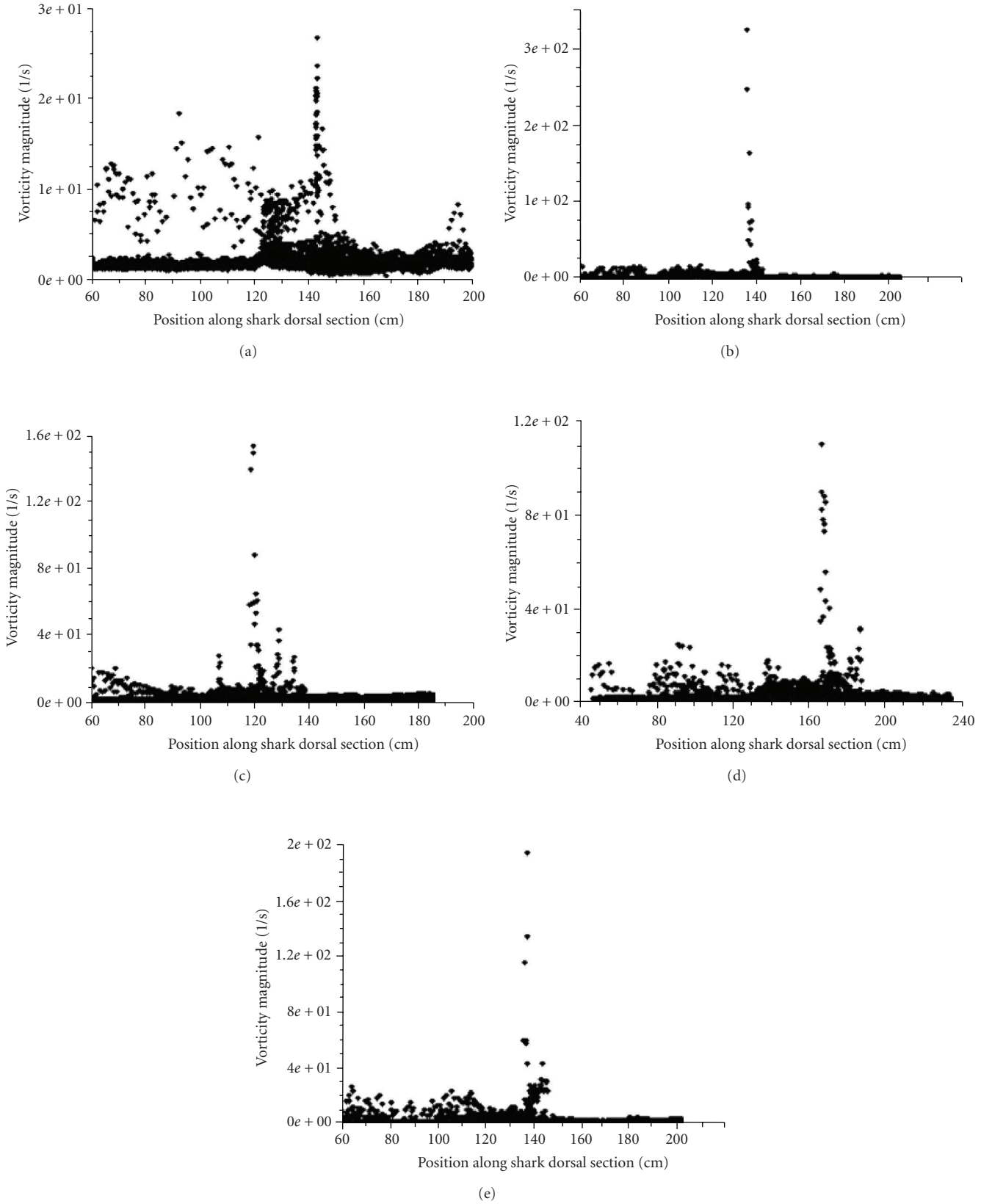

Figure 9: The vorticity magnitude on the body surface of the shark dorsal fin section models (a)–(e). The x-axis on the figure represents the y-axis along the shark dorsal section models and the y-axis shows the vorticity magnitude at every position on the shark at that particular y value. In this way, the figure shows the maximum vorticity magnitude at each position along the shark body model, clearly illustrating the vorticity spike at the dorsal fin trailing edge in each specimen.

swimming promote an optimisation of swimming efficiency in that particular mode. Morphological features such as eye sockets and gill slits were not included in the *P. glauca* models, as with the RoboTuna model [30]. Due to meshing inaccuracies the "v-notch" present on the dorsal side of *P. glauca* peduncles was not included in the shark models. This could induce microturbulence as suggested for chub mackerel (*Scomber japonicus*) finlets [34] and be of particular importance during active swimming due to its position just anterior to the caudal fin.

The change of flow regime achieved with removal of the dorsal fin was investigated using *Fluent* which models the flow around the sharks by solving Reynold averaged Navier-Stokes (RANSs) equations. The software encounters problems when modelling flow where viscous flow mechanisms dominate and nonlaminar (transition and turbulent) flow conditions are found [35]. Two-equation turbulent models reduce this error such as the k-epsilon model which is based on the turbulent kinetic energy (k) and the dissipation rate (ε) of k by viscosity. The use of RANS is known to produce a weakness in the prediction of flow separation but offers relatively stable turbulent flow regimes. The error in the turbulent flow caused by software limitations was taken into consideration by comparing the results from the shark models to flows along control cylinders using the same turbulent model.

Figure 9 shows a large vorticity maximum at the trailing edge of the dorsal fin on shark body models, along with a larger vorticity in the position of the dorsal fin. This suggests enhancement of dorsal fin-induced vorticity by the body morphology which is one of the three ways that Gopalkrishnan et al. [29] suggest in which the caudal fin could manipulate body produced vorticity (including annihilation and vortex pairing). An oscillating foil can be used to control oncoming vortices [36]. Sparenberg [13] described how manipulation of anterior vortices by the caudal fin during active swimming, particularly in subcarangiform swimming [37], could act to recover energy lost to the surrounding fluid in the form of kinetic energy. In this way the increased vorticity seen in shark body models shows the production of vortices which will become available for manipulation by the caudal fin. Further understanding of where these vortices form should assist in wake analysis and inform future investigations of fish swimming efficiency. The ability of *P. glauca* to control and manipulate vorticity would have evolutionary advantages in an environment where vortices are continuously created and dissipated on a number of different scales, including the wakes of other animals and through interaction with topology [4].

The flow modelled at the trailing edge of the dorsal fin will include an error due to the highly flexible free rear tip of the fin that would usually undergo deformations in hydrodynamic loading [10]. It is thought that deformations of the free rear tip would be minimal during coasting due to the straight posture assumed by the shark combined with hydrostatic pressure effects. A similar but much smaller error will be found around the dorsal fin which was also assumed to maintain rigidity (as in [10]). Further modelling studies for actively swimming *P. glauca* would need to include this free tip morphology to avoid inaccurate calculation of lateral forces from the dorsal fin. The inclusion of hydrostatic pressure effects will be more complex.

P. glauca body morphology was found to manipulate dorsal fin and body-induced vortices thereby increasing the mean vorticity regime around the shark in order to dissipate turbulent kinetic energy and reduce the velocity magnitude along the lateral line. It is suggested that the water flow is thus channelled along the lateral line in vortices in order to create a baseline flow to facilitate lateral line functionality particularly in the lower-frequency range and the ampullae of Lorenzini. A large relative velocity magnitude was found over the gill slits, due to anterior body morphology accelerating the flow thereby increasing oxygen uptake efficiency. In this way body morphology not only reduces drag due to annihilation of fin-induced turbulence but also increases the efficiency of *P. glauca* functional biology.

Acknowledgments

The authors gratefully acknowledge Dr. Steve Campana for permitting them to collect morphological measurements during the Nova Scotia shark derbies, 2007, and to Warren Joyce for assisting with a number of measurements.

References

[1] R. W. Blake, "Fish functional design and swimming performance," *Journal of Fish Biology*, vol. 65, no. 5, pp. 1193–1222, 2004.

[2] Q. Zhu, M. J. Wolfgang, D. K. P. Yue, and M. S. Triantafyllou, "Three-dimensional flow structures and vorticity control in fish-like swimming," *Journal of Fluid Mechanics*, vol. 468, pp. 1–28, 2002.

[3] I. K. Bartol, M. Gharib, D. Weihs, P. W. Webb, J. R. Hove, and M. S. Gordon, "Hydrodynamic stability of swimming in ostraciid fishes: role of the carapace in the smooth trunkfish *Lactophrys triqueter* (Teleostei: Ostraciidae)," *Journal of Experimental Biology*, vol. 206, no. 4, pp. 725–744, 2003.

[4] I. K. Bartol, M. Gharib, P. W. Webb, D. Weihs, and M. S. Gordon, "Body-induced vortical flows: a common mechanism for self-corrective trimming control in boxfishes," *Journal of Experimental Biology*, vol. 208, no. 2, pp. 327–344, 2005.

[5] J. E. Colgate and K. M. Lynch, "Mechanics and control of swimming: a review," *IEEE Journal of Oceanic Engineering*, vol. 29, no. 3, pp. 660–673, 2004.

[6] M. Narasimhan, H. Dong, R. Mittal, and S. N. Singh, "Optimal yaw regulation and trajectory control of biorobotic AUV using mechanical fins based on CFD parametrization," *Journal of Fluids Engineering*, vol. 128, no. 4, pp. 687–698, 2006.

[7] C. M. Breder, "The locomotion of fishes," *Zoologica*, vol. 4, pp. 159–256, 1926.

[8] P. W. Webb, "Body form, locomotion and foraging in aquatic vertebrates," *American Zoologist*, vol. 24, no. 1, pp. 107–120, 1984.

[9] M. Sfakiotakis, D. M. Lane, and J. B. C. Davies, "Review of fish swimming modes for aquatic locomotion," *IEEE Journal of Oceanic Engineering*, vol. 24, no. 2, pp. 237–252, 1999.

[10] T. Lingham-Soliar, "Caudal fin in the white shark, *Carcharodon carcharias* (Lamnidae): a dynamic propeller for fast,

efficient swimming," *Journal of Morphology*, vol. 264, no. 2, pp. 233–252, 2005.

[11] J. G. Casey and N. E. Kohler, "Long distance movements of Atlantic sharks from the NFS cooperative shark tagging programme," *Underwater Naturalist*, vol. 19, pp. 87–91, 1991.

[12] L. J. V. Compagno, *FAO Species Catalogue: Sharks of the World: An Annotated and Illustrated Catalogue of Shark Species Known to Date*, vol. 4 of *FAO Fisheries Synopsis 125*, Food & Agriculture Organization of the United Nations, Rome, Italy, 1984.

[13] J. A. Sparenberg, "Survey of the mathematical theory of fish locomotion," *Journal of Engineering Mathematics*, vol. 44, no. 4, pp. 395–448, 2002.

[14] N. Queiroz, F. P. Lima, A. Maia, P. A. Ribeiro, J. P. Correia, and A. M. Santos, "Movement of blue shark, *Prionace glauca*, in the north-east Atlantic based on mark-recapture data," *Journal of the Marine Biological Association of the United Kingdom*, vol. 85, no. 5, pp. 1107–1112, 2005.

[15] E. L. Brainerd and L. A. Ferry-Graham, "Mechanics of respiratory pumps," in *Fish Biomechanics*, R. E. Shadwick and G. V. Lauder, Eds., vol. 23 of *Fish Physiology*, pp. 1–28, Elsevier Academic Press, San Diego, Calif, USA, 2006.

[16] K. P. Maruska, "Morphology of the mechanosensory lateral line system in elasmobranch fishes: ecological and behavioral considerations," *Environmental Biology of Fishes*, vol. 60, no. 1–3, pp. 47–75, 2001.

[17] A. J. Kalmijn, "Electric and magnetic sensory world of sharks, skates and rays," in *Sensory Biology of Sharks, Skates and Rays*, E. S. Hodgson and R. F. Mathewson, Eds., pp. 507–528, US Government Printing Office, Washington, DC, USA, 1978.

[18] R. E. Hueter, D. A. Mann, K. P. Maruska, J. A. Sisneros, and L. S. Demski, "Sensory biology of elasmobranchs," in *Biology of Sharks and Their Relatives*, J. C. Carrier, J. A. Musick, and M. R. Heithaus, Eds., pp. 325–368, CRC Press, Boca Raton, Fla, USA, 2004.

[19] J. C. Montgomery, C. F. Baker, and A. G. Carton, "The lateral line can mediate rheotaxis in fish," *Nature*, vol. 389, no. 6654, pp. 960–963, 1997.

[20] D. M. Higgs, Z. Lu, and D. A. Mann, "Hearing and mechanoreception," in *The Physiology of Fishes*, D. H. Evans and J. B. Claiborne, Eds., pp. 389–428, CRC Press, Boca Raton, Fla, USA, 3rd edition, 2006.

[21] S. Coombs and S. van Netten, "The hydrodynamics and structural mechanics of the lateral line system," in *Fish Biomechanics*, R. E. Shadwick and G. V. Lauder, Eds., vol. 23 of *Fish Physiology*, pp. 103–140, Elsevier, San Diego, Calif, USA, 2006.

[22] W. Raschi and C. Tabit, "Functional aspects of placoid scales: a review and update," *Australian Journal of Marine & Freshwater Research*, vol. 43, pp. 123–147, 1992.

[23] S. E. Campana, L. Marks, W. Joyce, and N. E. Kohler, "Effects of recreational and commercial fishing on blue sharks (*Prionace glauca*) in Atlantic Canada, with inferences on the North Atlantic population," *Canadian Journal of Fisheries and Aquatic Sciences*, vol. 63, no. 3, pp. 670–682, 2006.

[24] G. L. Wood, *The Guinness Book of Animal Facts and Feats*, G. L. Woods and Guinness Superlatives, New York, NY, USA, 1982.

[25] L. F. Sundström, S. H. Gruber, S. M. Clermont, et al., "Review of elasmobranch behavioral studies using ultrasonic telemetry with special reference to the lemon shark, *Negaprion brevirostris*, around Bimini Islands, Bahamas," *Environmental Biology of Fishes*, vol. 60, no. 1–3, pp. 225–250, 2001.

[26] S. A. Wainwright, F. Vosburgh, and J. H. Hebrank, "Shark skin: function in locomotion," *Science*, vol. 202, no. 4369, pp. 747–749, 1978.

[27] E. J. Anderson, W. R. McGillis, and M. A. Grosenbaugh, "The boundary layer of swimming fish," *Journal of Experimental Biology*, vol. 204, no. 1, pp. 81–102, 2001.

[28] G. Vaz, R. Van der Wal, C. Mabilat, and P. Gallagher, "Viscous flow computations on smooth cylinders a detailed numerical study with validation," in *Proceedings of the 26th International Conference on Offshore Mechanics and Arctic Engineering (OMAE '07)*, vol. 3, pp. 849–860, San Diego, Calif, USA, June 2007.

[29] R. Gopalkrishnan, M. S. Triantafyllou, G. S. Triantafyllou, and D. Barrett, "Active vorticity control in a shear flow using a flapping foil," *Journal of Fluid Mechanics*, vol. 274, pp. 1–21, 1994.

[30] D. S. Barrett, M. S. Triantafyllou, D. K. P. Yue, M. A. Grosenbaugh, and M. J. Wolfgang, "Drag reduction in fish-like locomotion," *Journal of Fluid Mechanics*, vol. 392, pp. 183–212, 1999.

[31] U. K. Müller and J. L. Van Leeuwen, "Undulatory fish swimming: from muscles to flow," *Fish and Fisheries*, vol. 7, no. 2, pp. 84–103, 2006.

[32] D. Bernal, K. A. Dickson, R. E. Shadwick, and J. B. Graham, "Review: analysis of the evolutionary convergence for high performance swimming in lamnid sharks and tunas," *Comparative Biochemistry and Physiology*, vol. 129, no. 2-3, pp. 695–726, 2001.

[33] J. M. Donley, C. A. Sepulveda, P. Konstantinidis, S. Gemballa, and R. E. Shadwick, "Convergent evolution in mechanical design of lamnid sharks and tunas," *Nature*, vol. 429, no. 6987, pp. 61–65, 2004.

[34] J. C. Nauen and G. V. Lauder, "Locomotion in scombrid fishes: morphology and kinematics of the finlets of the chub mackerel *Scomber japonicus*," *Journal of Experimental Biology*, vol. 203, no. 15, pp. 2247–2259, 2000.

[35] R. Mittal, "Computational modeling in biohydrodynamics: trends, challenges, and recent advances," *IEEE Journal of Oceanic Engineering*, vol. 29, no. 3, pp. 595–604, 2004.

[36] M. M. Koochesfahani and P. Dimotakis, "A cancellation experiment in a forced turbulent shear layer," in *Proceedings of the 1st National Fluid Dynamics Congress*, pp. 1204–1208, Cincinnati, Ohio, USA, July 1988.

[37] M. J. Lighthill, *Mathematical Biofluid Dynamics*, SIAM, Philadelphia, Pa, USA, 1975.